Journal of Physics and Chemistry of Solids 71 (2010) 119–124

Contents lists available at ScienceDirect

Journal of Physics and Chemistry of Solids

journal homepage: www.elsevier.com/locate/jpcs

# Oxidation of nanocrystalline aluminum by variable charge molecular dynamics

A. Perron [a], S. Garruchet [a], O. Politano [a,*], G. Aral [b], V. Vignal [a]

[a] Département Interface et Réactivité dans les Matériaux, Institut Carnot de Bourgogne, UMR 5209 CNRS-Université de Bourgogne, 9 AV. Alain Savary, BP 47870, 21078 DIJON Cedex, France

[b] Institut of Physics, Izmir Institut of Technology, Gulbahce Campus, TR-35437, Urla, Izmir, Turkey

ARTICLE INFO

*Article history:*
Received 29 May 2009
Received in revised form
14 September 2009
Accepted 15 September 2009

*Keywords:*
A. Metals
A. Oxides
A. Thin films
D. Diffusion
D. Microstructure

ABSTRACT

We investigate the oxidation of nanocrystalline aluminum surfaces using molecular dynamics (MD) simulations with the variable charge model that allows charge dynamically transfer among atoms. The interaction potential between atoms is described by the electrostatic plus (Es+) potential model, which is composed of an embedded atom method potential and an electrostatic term. The simulations were performed from 300 to 750 K on polycrystalline samples with a mean grain size of 5 nanometers. We mainly focused on the effect of the temperature parameter on the oxidation kinetic. The results show that, beyond a first linear regime, the kinetics follows a direct logarithmic law (governed by diffusion process) and tends to a limiting value corresponding to a thickness of ~3 nm. We also characterized at 600 K the effects of an external applied strain on the microstructure and the chemical composition of oxide films formed at the surface. In particular, we obtained a partially crystalline oxide films for all temperatures and we noticed a strong correlation between the degree of crystallinity of the oxide film and the oxidation temperature.



## 1. Introduction

Metal/oxide interfaces play critical roles in many applications, such as structural or functional materials in materials science, microelectronics, chemical and biomedical applications. In materials science for instance, the following technological materials are based on metal/oxide interfaces: functional ceramics with metals (cermets), oxide dispersion-strengthened alloys, oxide coatings on metals functioning as thermal barriers or natural corrosion protection layers. This is in particular the case of oxide passive films formed spontaneously on aluminum and aluminum alloys, which protect the surface against further oxidation and corrosion. Also, because of their specific physical properties (i.e. large dielectric constant and height barrier for electron tunneling), aluminum oxides are promising candidate for gate dielectrics in the nanoscale CMOS technology, magnetic tunneling junctions, magnetic sensors, magnetic storage devices and solid-state memory, etc. [1–3]. At the same time, significant progress has been made to understand the combustion of nanoaluminum powders and the highly exothermic reaction of fine-grained aluminum particles (size $< 100$ nm) with oxygen because of their use as potential additives to propellants for rockets [4–9]. For all these applications, it is crucial to understand the physico-chemical processes, which control the reactivity of the metallic substrate and the thickness, morphology, chemical composition and microstructure of the oxide film [1].

The development of numerical studies of metal/oxides interfaces as well as oxide growth on the top of metals have required the development of a new class of interaction potential such as, for example, the variable charge method proposed by Streitz and Mintmire [10], which is often referred as the (Es+) potential. This last combines an embedded atom method (EAM) potential and an electrostatic term to model the metal–metal, oxygen–oxygen and metal–oxygen interactions. The EAM contribution is predominant in the metallic region whereas the coulombic potential is used to model the ionic interactions within the oxide. It was initially fitted to model several properties of metallic aluminum (Al) and alpha alumina ($\alpha$-$Al_2O_3$), which is the only thermodynamically stable Al oxide. Later, Streitz and Mintmire [11] also showed that the (Es+) potential was able to describe the gamma alumina ($\gamma$-$Al_2O_3$) structure with a reasonable degree of accuracy. This last point is of importance in the framework of the present study as high temperature oxidation of aluminum usually leads to the formation of transition alumina depending on the temperature.

Initially designed to simulate the properties of one metal (namely Al) interacting with oxygen, the Streitz and Mintmire potential was recently extended/modified to simulate many metals (Ti, Zr, Fe, Ni, Co, etc) and alloys [12–18]. It was used to

* Corresponding author. Tel.: +33 0 380 39 6172; fax: +33 0 380 39 6132.
*E-mail address:* olivier.politano@u-bourgogne.fr (O. Politano).

0022-3697/$ - see front matter © 2009 Elsevier Ltd. All rights reserved.
doi:10.1016/j.jpcs.2009.09.008

study nanocrystalline metal-oxide properties [16–18] or processes involved in the oxidation of metallic substrates [12,13,19–22]. In this last case, the capability of the interatomic potential to determine the atomic charges on atoms due to its local environment was used to model the chemical reactions (bond formation and bond breakage) between a metal and an oxygen gas within a molecular dynamics simulation.

Recently, a new approach [23] was developed to solve one deficiency of the afore-mentioned variable charge models, which were found to weakly describe the iono-covalent nature of the metal–oxygen bonding. For example, they lead to underestimation by 30% of the calculated formation energy of an oxygen vacancy. This new generation of variable charge models incorporates new physics through a tight binding analytical model [24] and gave very satisfactory results for $ZrO_2$ and $TiO_2$ polymorphs. It looks very promising for the development of the future simulation of metal/oxide systems.

Oxidation of Al nanoclusters [19,20] or single-crystal surfaces of Al [21,22] for pressure ranging from 10 to 40 times the normal state were studied by variable charge molecular dynamics (VCMD) approaches. Under their oxidation conditions, these works clearly characterized the formation of an amorphous oxide layer. They reported a growth mechanism proceeding by both anionic and cationic diffusions and a direct logarithm relationship for the oxidation kinetic. Note that these VCMD simulations never permit to characterize the formation of a well crystalline oxide film.

On the other hand, experimental investigations on the high temperature oxidation of pure aluminum surfaces are difficult to perform due to the very high reactivity of Al with O and the presence of the native protective alumina scale. Surface preparation under high vacuum conditions is required and in-situ experimental techniques have to be conducted under very low oxidation pressure. Many experiments on bulk aluminum surfaces were developed by Jeurgens et al. with XPS and Auger spectroscopy. These studies were performed at very low oxidation pressure ($\sim 10^{-4}$ Pa) and mainly focused on the reaction kinetic, the composition and the structure of the alumina scale as a function of the temperature. That is (i) at low temperatures ($T < 573$ K), an amorphous and Al-deficient (as compared to $\gamma$-$Al_2O_3$) thin oxide film ($< 5$ nm) is formed; (ii) at higher temperatures ($T \geq 673$ K), during the initial fast oxidation stage an Al-enriched amorphous oxide film is obtained and during the second slow oxidation stage the films gradually reach the stoichiometric composition and the crystalline structure of $\alpha$-$Al_2O_3$ [25–29].

In the present approach, we studied the oxidation under a constant molecular oxygen density (1 atm) of a polycrystalline Al substrate with a mean grain size of 5 nm. We focused on the relation between the growth kinetics and the evolution of the chemical composition, by studying the structure of the developing oxide scale. In order to compare with the existing experimental results of Jeurgens et al., we used the same range of oxidation temperature (i.e., 300, 600 and 750 K). Moreover, to highlight the influence of an applied strain on the oxidation mechanisms, one atomistic system was oxidized at 600 K after a uniaxial deformation (+7%).

## 2. Computational methods

We used the variable charge molecular dynamics method (VCMD) originally proposed by Streitz and Mintmire [10] for Al–O systems. In this formalism, the inter-atomic potential is a sum of the electrostatic and Finnis–Sinclair embedded atom potentials and allows the atomic charges to vary dynamically in response to changes in the local environment of the atoms. The variable charge approach determines atomic charges at each molecular dynamic step in such a way that the electrostatic potential energy is minimized, with the charge-neutrality constraint, i.e. the sum of the atomic charges is equal to zero. This condition is equivalent to the electronegativity equalization principle, which requires that each atoms, aluminum (Al) and oxygen (O), have an equal chemical potential.

The VCMD code used in this approach is developed by the "Collaboratory for Advanced Computing and Simulations" group at the University of Southern California [20]. It is highly parallel and allows simulating of million atoms metal-oxide systems. To speedup calculations, state of the art techniques are implemented: multiple time steps, multilevel preconditioned conjugate gradient method, fast multipole method and domain decomposition approach are used to implement the MD algorithm on parallel architectures [30–32].

The initial Al polycrystalline sample is a cube of size 10.256 nm containing 62 932 atoms. The bulk polycrystalline system was created at 0 K by using a procedure analogous to the one used to obtain Voronoi cells (Fig. 1a). It was then thermalized by successive jumps of 50 K until the desired temperature using Noose–Hoover thermostat chain [33]. The slab geometry is then created by incorporating in the simulation box two vacuum slabs along the $Z$-direction while periodic boundary conditions are imposed along $X$ and $Y$-axis. For more details about the sample preparation procedure, the reader should refer to [34]. The final dimension of the simulation box is $Z = 15$ nm and $X = Y = 10.256$ nm (Fig. 1b). Our MD simulations were performed using a constant oxygen molecular density equal to the normal state $P^0$ (1 atm) above the Al polycrystalline surface. Every MD steps, the number of oxygen atoms present in the gas is examined and if this number is less than the imposed value, then new oxygen molecules (with a velocity equal to the oxidation temperature) are randomly introduced into the region above the Al surface in order to maintain the molecular oxygen density constant.

During the oxidation stage, only Al atoms belonging to the lower 0.7 nm part of the polycrystalline substrate (Fig. 1b) were kept thermalized using the thermostat. The constrain on the other Al atoms was removed and their kinetic energy (temperature) was free to evolve during all the oxidation process [35].

We integrated the equation of motions using a multiple time step algorithm in which the MD time step is $dt = 1$ fs for short-range forces and $dt = 5$ fs for long-range forces. As the calculation of charges is the most consuming part of VCMD, the local atomic charges are only calculated every 100th time steps. That is, after their updates the charges are kept constants during the following 99 steps to compute the forces and energies. A cutoff radius of 0.6 nm was used to compute the Finnis–Sinclair potential.

The strain samples were created by following a procedure, which gave satisfactory results to study the multilayer surface relaxation of Al single-crystals [36] or the formation of surface roughness on strained polycrystalline Al substrates [34]. It consists of a direct deformation of the sample to the desired length. That is, we rescaled instantaneously the positions of the atoms along the $Y$-direction in order to obtain the required strain. The sample was then relaxed during 50 ps.

## 3. Results and discussion

### 3.1. Kinetic law

The kinetic curves obtained for all systems (unstrained: 300, 600 and 750 K; strained: 600 K) are plotted on Fig. 2. In this figure, the $y$-axis represents the evolution of the number of oxygen atoms

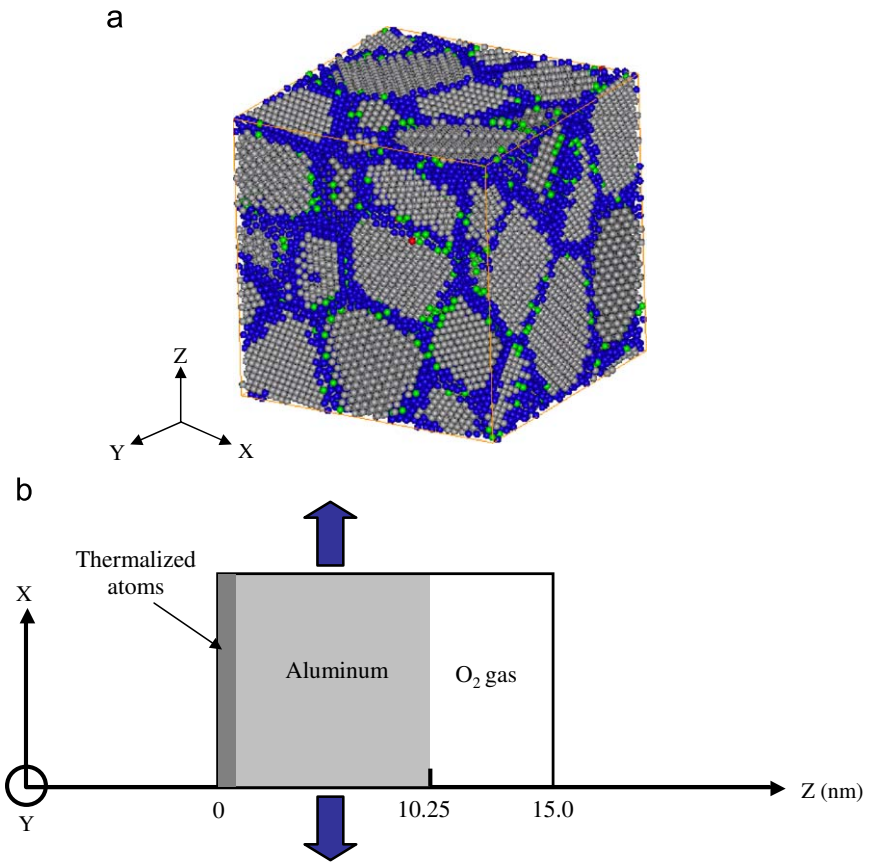


**Fig. 1.** (a) Bulk polycrystalline aluminum sample composed of 62 969 atoms. The grey light atoms correspond to the grains and the dark grey to the grain boundaries. (b) Schematic representation of the simulation box, which contains aluminum slab and $O_2$ gas. The arrows indicate the loading direction (uniaxial deformation, +7%).

introduced into the simulation box per unit surface area ($nm^2$). It can be assimilated to the variation of sample weight measured experimentally (Fig. 2a). The thickness of the oxide film is determined by calculating the difference between the mean position in the *Z*-direction of the ten highest Al atoms (near the gas/oxide interface) and the ten deepest oxygen atoms (at the metal/oxide interface). As one can notice, Figs. 2a and b are similar to the classical representations obtained during high temperature oxidation experiments: sample weight gain/loss and film thickness evolution.

The kinetic curves presented in Fig. 2a show identical behaviors for all oxidizing conditions. They can be divided into two parts: a first linear law followed by a direct logarithmic relationship. According to the oxidation theory and heterogeneous kinetics [37–40], during the linear part the interfacial processes (dissociation of oxygen molecules, sorption of oxygen atoms and Al–O reaction) are predominant. Indeed, at the beginning of the oxidation, the oxygen atoms react directly with Al substrate and the rate of this reaction governs the global kinetic. As presented in Fig. 2a, the linear law is available until around 1 ns of oxidation and corresponds to an oxide thickness of ~1.5 nm (Fig. 2b). After this point, the oxygen atoms do not have direct access to Al substrate but at first have to cross the oxide film, which acts as a barrier. So, this second kinetic part of the oxidation is controlled by diffusion of atomic species (oxygen and aluminum) through the film.

As two different processes occur during oxidation, we analyzed the kinetic curves using a comprehensive law combining linear and logarithmic/exponential terms:

$$t = \frac{1}{K_l}(N/S) + \frac{1}{D}\left(10^{\frac{N}{S*K_{log}}} - E\right) \quad (1)$$

In this expression, $t$ is the oxidation time, $N/S$ is the number of oxygen atoms per unit area in the oxide film, $K_l$ and $K_{log}$ are the linear and logarithmic constants, respectively and $D$ and $E$ are the mathematical parameters. Such combination of kinetic laws is rather standard when different processes occur during oxidation (the best example is the well-known linear-parabolic relationship) and is detailed in textbooks on high temperature oxidations [37–40].

The numerical fitting of kinetic curves using Eq. (1) is reported in Fig. 3. We can observe an excellent fit of the oxidation kinetic by the comprehensive law: for low values of $N$, the linear law is predominant and then, with increase in $N$, the logarithmic law becomes majority. The parameters obtained from the numerical fitting are given in Table 1. As one can notice, $K_l$, which is the slope of the linear part remains almost constant for all oxidizing conditions. Therefore, sorption phenomena of oxygen are not modified by oxidation temperature or applied strain. On the other hand, $K_{log}$ increases with temperature and applied strain. Therefore, the diffusion of atomic species is facilitated by increasing the motion of atoms (temperature) and the interatomic distances (deformation). The activation energy, which can be deduced from the Arrhenius plots ($\ln(K_{log}$ ) versus $1/T$), was estimated at 1.3 kJ $mol^{-1}$. This value is rather low compared to experimental results ranging from 9.5 to 238 kJ $mol^{-1}$ for the oxidation of bulk Al or nanoparticles (~50 nm) [7–9]. This difference might be explained by the very high reactivity of our samples induced by their small nanocrystalline microstructure (5 nm grains), their total purity and the absence of a protective alumina scale at the surface of the sample. Finally, we note that the growth processes proceed almost exclusively by anionic migration (internal movement of oxygen anions through the oxide to the metal substrate).

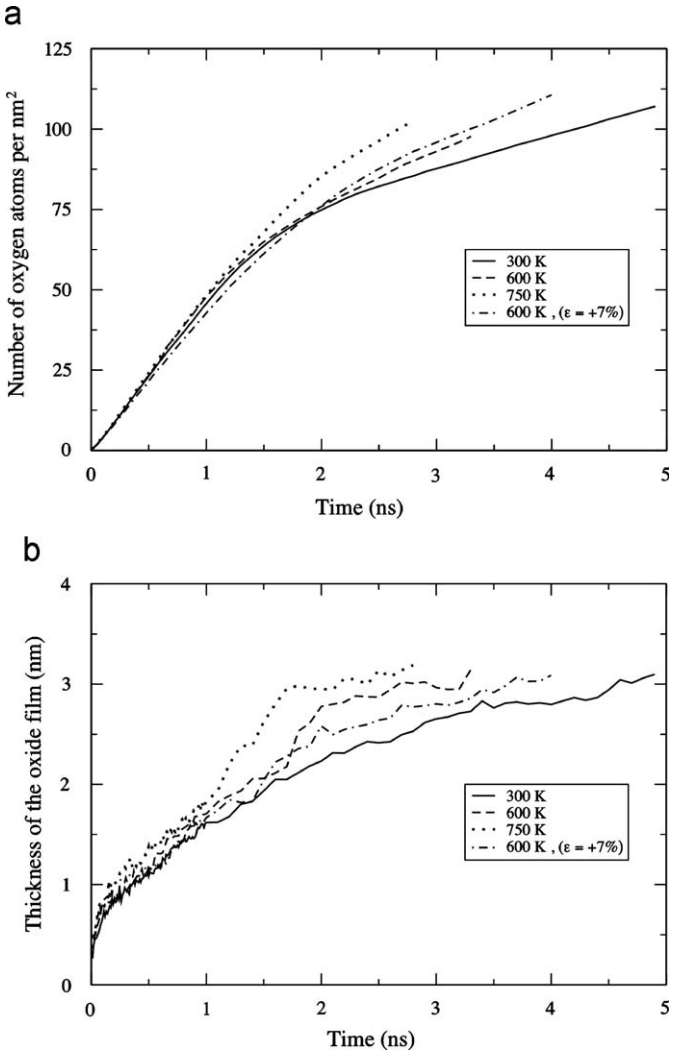


**Fig. 2.** (a) Evolution of the number of oxygen atoms consumed by the oxidation process and (b) of the thickness of the oxide film in function of time, temperature and applied strain.

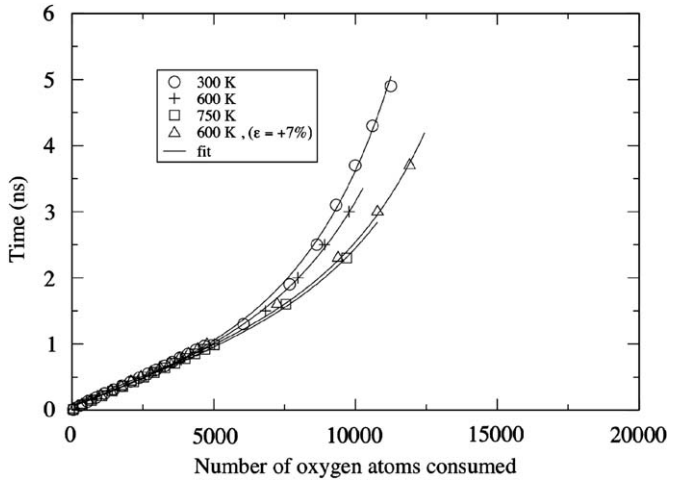


**Fig. 3.** Oxidation time as a function of the number of oxygen atoms. The symbols are the results from the simulations. The straight lines are the fit with the comprehensive logarithmic law (straight line) for each oxidation condition.

**Table 1**
Parameters values of the comprehensive law according to the oxidation temperature and applied strain.

| | $K_l$ (atoms nm$^{-2}$ ps$^{-1}$) | $D$ (ps$^{-1}$) | $K_{log}$ (atoms nm$^{-2}$) | $E$ |
|---|---|---|---|---|
| 300 K | 0.0634 | 0.0209 | 57.4320 | 0.00932 |
| 600 K | 0.0655 | 0.0197 | 62.2611 | 0.02868 |
| 750 K | 0.0634 | 0.0133 | 85.6410 | 0.4500 |
| 600 K ± 7% | 0.0592 | 0.0126 | 76.588 | 0.3095 |

**Table 2**
Evolution of atomic fractions and atomic densities in oxide films formed at 300, 600 and 750 K, and after deformation (+7%).

| | 300 K | 600 K | | 750 K |
|---|---|---|---|---|
| Applied strain | 0% | 0% | $\varepsilon_X$ = +7% | 0% |
| Al atomic fraction in the oxide film | 0.50 | 0.53 | 0.51 | 0.52 |
| O atomic fraction in the oxide film | 0.50 | 0.47 | 0.49 | 0.48 |
| Aluminum atomic density (atoms nm$^{-3}$) | 49.8 | 49.1 | 49.2 | 48.5 |
| Oxygen atomic density (atoms nm$^{-3}$) | 49.0 | 43.5 | 47.3 | 44.7 |
| Total atomic density (atoms nm$^{-3}$) | 98.8 | 92.6 | 96.5 | 93.2 |

The presence of the two kinetic regimes is corroborated by previous studies from Hasnaoui et al. [21,22] on the oxidation of single-crystal Al surfaces. Indeed, these authors mentioned a short "transition" initial stage before the direct logarithmic law. Based on the present work, we are now able to conclude that the "transition" stage observed by Hasnaoui et al. was linear and governed by interfacial processes.

Concerning the oxide film thickness represented on Fig. 2b, we can observe an increase with the temperature until ~3 nm. This agrees well with the value of 5 nm reported by Jeurgens et al. [27] with in-situ XPS and Auger spectroscopy. Furthermore, small variations in thickness are observed after 1 ns for 600 and 750 K. We observed a layer by layer growth mode for the oxide film at 300 K. At higher temperature, the growth of the oxide is less uniform and leads to fluctuations observed in Fig. 2b. Furthermore, microstructural changes in the oxide film can also produce this behavior. This last will be developed in the next section.

### 3.2. Chemical composition

As suggested above, the morphology and the composition of oxide films seem to vary with the temperature. To clarify the changes in composition, the fractions of aluminum, oxygen atoms and various atomic densities have been calculated at the end of each oxidation. In order to avoid any spurious effect due to the interfaces, which are too concentrated in aluminum or oxygen atoms, the calculations are performed between 0.5 nm under the oxide/gas limit and 0.5 nm above the substrate/oxide limit. It corresponds to the middle part of the oxide film. The obtained values are reported in Table 2 and are discussed below.

Concerning the temperature, an increase in the aluminum atomic fraction in the oxide film is observed between 300 and 600 K (and consequently a proportional decrease in the oxygen fraction). Moreover, the Al atomic density decreases slightly with temperature whereas the O atomic density decreases strongly. As a consequence, the total density is decreasing between 300 and 600 K. To resume, the increase in the oxidation temperature induces an increase in the kinetic law and produces oxide films, which are less dense and enriched in Al. Concerning the oxide film formed at 750 K, the composition is similar to the one formed at 600 K but the density is different. It indicates that the microstructure changed between 600 and 750 K. This point will be studied in more detail afterwards.

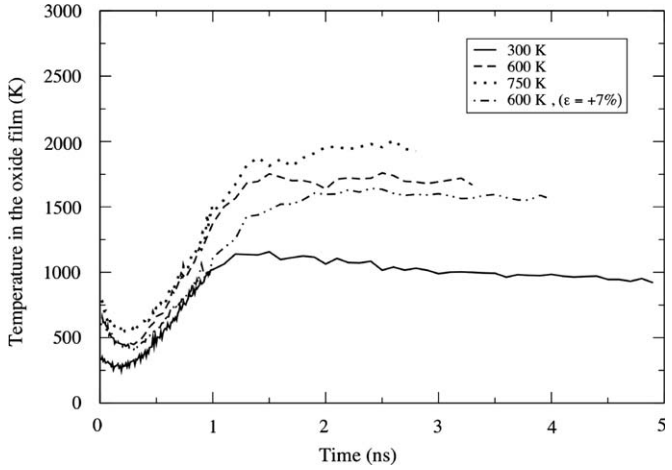


**Fig. 4.** Temperature of the oxide film formed as a function of time for different oxidation temperatures (300, 600 and 750 K) and straining conditions (+7%).

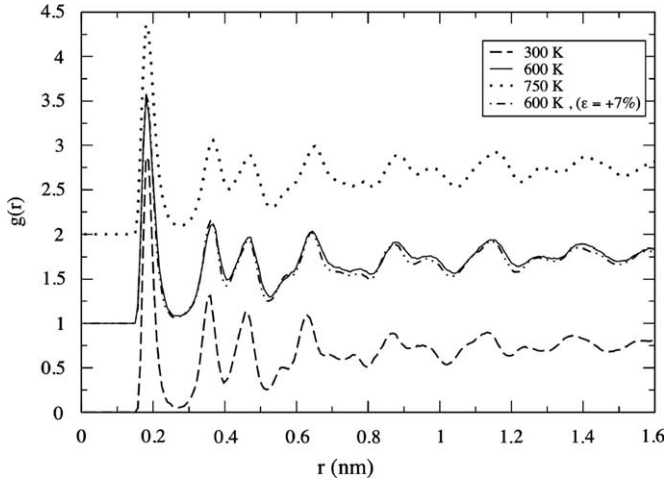


**Fig. 5.** Pair distribution function, g(*r*), for the Al–O interatomic distances in the middle part of the oxide films.

Concerning the applied strain (+7%): we noticed a slight increase in the O fraction and a strong increase in the O atomic density in the oxide film. In our point of view, these observations are due to the increase in the inter-atomic distances (Al–Al), which facilitates the insertion of O atoms in the substrate.

### 3.3. Microstructure characterizations

The temperature of the oxide film was computed as a function of time and is shown in Fig. 4. First, we observed a slight decrease in the temperature until the oxide scale covers completely the surface. After this very short transition regime, a great increase in the temperature in the oxide is observed until ~1.5 ns. This phenomenon corresponds to the linear kinetic law determined previously (sorption process). After 1.5 ns, which corresponds to the beginning of the logarithmic kinetic law (diffusion processes), the temperature of the oxide films reaches a maximum and then decreases very slowly with time. So, the evolution of the oxide temperature can be associated with the number of oxygen consumed. The oxidation reaction of Al is highly exothermic ($-1675\,kJ\,mol^{-1}$) and, therefore, leads to a great increase in the oxide film temperature (included between 1000 and 2000 K). These high temperatures will favor the formation of crystalline $Al_2O_3$ structures as it increases the atomic motion/rearrangement in the films.

Pair distribution functions (PDF) for the Al–O bonds have been calculated in the middle part of the oxide films in order to characterize their microstructure. As presented in Fig. 5, many peaks are observed on the PDF and indicate the presence of long-range order (a partially crystalline structure). But, no clear difference can be seen between the different curves. Moreover, one cannot determine the crystalline microstructure of films from Fig. 5. A second step consists in calculating the environment of each atom by applying a common neighbor analysis on Al and O atoms [41,42]. The crystallographic structure of the thermodynamically stable alumina ($\alpha$-$Al_2O_3$) is based on a hexagonal network of O and Al atoms [43]. Therefore, as a first approach we used the percentage of oxygen atoms located in the hexagonal compact position (hcp) within the oxide as a criteria to characterize the crystallinity of the film formed at the Al surface. The results are reported in Table 3. As one can see, the percentage of O in hcp positions increases with temperature and also by applying a strain on the metallic substrate. This last highlights an increase in the degree of crystallinity from ~32% at 300 K to ~43% at 750 K. Finally, the change in the microstructure between 600 and 750 K suggested previously is confirmed. However, many transition alumina exist—γ, η (cubic), θ, θ′, θ″, λ (monoclinic), δ-$Al_2O_3$ (tetragonal or orthorhombic), α (trigonal), κ (orthorhombic), χ (hexagonal)—and the present study did not allowed us to determine which alumina polymorphs is present. In a forthcoming study, a more extended quantification of the ratios of tetrahedral $AlO_4$ and octahedral $AlO_6$ units will certainly help us to determine which alumina polymorph is formed during the simulation.

**Table 3**
Percentage of oxygen atoms in hexagonal compact position within the oxide layer.

| Conditions | 300 K | 600 K | 750 K | 600 K—strained |
|---|---|---|---|---|
| Degree of crystallinity (in %) | 31.7 | 37.6 | 41.5 | 42.5 |

Concerning the polycrystalline microstructure, we did not observed a significant difference in the reactivity between Al atoms located in grains or in grains boundaries. Also, no preferential diffusion of the oxygen ions was observed at the grain boundaries.

## 4. Conclusion

We performed VCMD simulations on the oxidation of nano-crystalline aluminum between 300 and 750 K. The influence of an external applied strain was also studied at 600 K. This last permit us to obtain the corresponding kinetic curves and the formation of a thin oxide film, which was analyzed with a common neighbor analysis and with pair distribution functions. The kinetic curves show the formation of a film with a limited thickness of about 3 nm. Those curves can be divided into two regimes: a linear and a logarithmic. According to heterogeneous kinetics, these two regimes are governed by interfacial processes and diffusion, respectively. A comprehensive kinetic relationship permits us to compute the linear and logarithmic constants. The linear constant was found to be independent of the temperature and the applied strain. On the contrary, the logarithmic constant, related motion of the atoms in the oxide scale, increases with both temperature and strain. Also, an increased in the degree of crystallinity within the oxide was observed with temperature and strains. We did not observe any preferential diffusion at the grain boundaries in the polycrystalline substrate.

Moreover, it is important to note that previous MD studies on single-crystal aluminum samples only reported the formation of amorphous alumina films. Here, we obtained the formation of a partially crystalline structure (42% of O atoms in hcp positions at 750 K). To our opinion, this might be related to the lower oxygen pressure ($P$=1 atm) used in the present approach as well as in the use of a large surface area, which reduces the border effects. Also the kinetic factor is crucial and in order to leave the atoms reorganize to obtain a well crystalline oxide, we will surely have to simulate much longer times.

## Acknowledgments

The authors want to thanks P. Vashishta, A. Nakano and R. Kalia for fruitful discussions. This work has been partially performed under the HPC-EUROPA (RII3-CT-2003-506079) with the support of the European Community-Research Infrastructure Action under the FP6 "structuring the European Research Area Progamme". Part of computations have been carried out at the CRI-CCUB, IDRIS and ULAKBIM high performance computing center.

## References

[1] J.M. De Teresa, A. Barthelemy, A. Fert, et al., Science 286 (1999) 507.
[2] E.S. Snow, P.M. Campbell, R.W. Rendell, et al., Semicond. Sci. Technol. 13 (1998) A75.
[3] A.T.M. van Gogh, S.J. van der Molen, J.W.J. Kerssemakers, et al., Appl. Phys. Lett. 77 (2000) 815.
[4] A. Rai, K. Park, L. Zhou, et al., Combust. Theor. Model. 10 (2006) 843.
[5] A.L. Ramaswamy, P. Kaste, Energ. Mater. 23 (2005) 1.
[6] S. Alavi, J.W. Mintmire, D.L. Thompson, J. Phys. Chem. 109 (2005) 209.
[7] J.M. Aaron, H.M. Chanb, M.P. Harmer, et al., J. Eur. Ceram. Soc. 25 (2005) 3413.
[8] K. Park, D. Lee, A. Rai, et al., J. Phys. Chem. B 109 (2005) 7290.
[9] F.H. Lu, H.D. Tsai, Y.C. Chieh, Thin Solid Films 516 (2008) 1871.
[10] F.H. Streitz, J.W. Mintmire, Phys. Rev. B 50 (1994) 11996.
[11] F.H. Streitz, J.W. Mintmire, Phys. Rev. B 60 (1999) 773.
[12] X.W. Zhou, H.N.G. Wadley, J.S. Filhol, et al., Phys. Rev. B 69 (2004) 035402.
[13] X.W. Zhou, H.N.G. Wadley, J. Phys.: Condens. Matter 17 (2005) 3619.
[14] S. Ogata, H. Lyetomi, K. Tsuruta, et al., J. Appl. Phys. 86 (1999) 3036.
[15] A. Hallil, R. Tétot, F. Berthier, et al., Phys. Rev. B 73 (2006) 165406.
[16] V. Tomar, M. Zhou, Phys. Rev. B 73 (2006) 174116.
[17] A. Elsener, O. Politano, P.M. Derlet, et al., Modelling Simulation. Mater. Sci. Eng. 16 (2008) 025006.
[18] A. Elsener, O. Politano, P.M. Derlet, et al., Acta Mater. 57 (2009) 1988.
[19] T. Campbell, R.K. Kalia, A. Nakano, et al., Phys. Rev. Lett. 82 (1999) 4866.
[20] T.J. Campbell, G. Aral, S. Ogata, et al., Phys. Rev. B 71 (2005) 205413.
[21] A. Hasnaoui, O. Politano, J.M. Salazar, et al., Surf. Sci. 579 (2005) 47.
[22] A. Hasnaoui, O. Politano, J.M. Salazar, et al., Phys. Rev. B 73 (2006) 035427.
[23] R. Tétot, A. Hallil, J. Creuze, et al., EPL 83 (2008) 40001.
[24] J. Goniaski, C. Noguera, Surf. Sci. 319 (1994) 81.
[25] L.P.H. Jeurgens, W.G. Sloof, F.D. Tichelaar, et al., Surf. Sci. 506 (2002) 313.
[26] L.P.H. Jeurgens, W.G. Sloof, F.D. Tichelaar, et al., Thin Solid Films 418 (2002) 89.
[27] L.P.H. Jeurgens, W.G. Sloof, F.D. Tichelaar, et al., J. Appl. Phys. 92 (2002) 1649.
[28] P.C. Snijders, L.P.H. Jeurgens, W.G. Sloof, Surf. Sci. 496 (2002) 97.
[29] P.C. Snijders, L.P.H. Jeurgens, W.G. Sloof, Surf. Sci. 589 (2005) 98.
[30] M. Tuckerman, B.J. Berne, G.L. Martyna, J. Chem. Phys. 97 (1992) 1990.
[31] A. Nakano, Comput. Phys. Commun. 104 (1997) 59.
[32] L. Greengard, V. Rokhlin, J. Comp. Phys. 73 (1987) 325.
[33] D. Frenkel, B. Smith, Understanding Molecular Simulation, Academic Press, San Diego, 2002.
[34] A. Perron, O. Politano, V. Vignal, Philos. Mag. 87 (2007) 129.
[35] A. Perron, Apport de la dynamique moléculaire et de techniques expérimentales à une échelle locale pour l'étude de surfaces d'aluminium déformées et/ou oxydées, Thèse de doctorat-Université de Bourgogne, 2008.
[36] O. Politano, S. Garruchet, J.M. Salazar, Mat. Sci. Eng. A 387–389 (2004) 749.
[37] N. Birks, G.H. Meier, Frederick S. Pettit, Introduction to the High-Temperature Oxidation of Metals, second ed., Cambridge University Press, 2006.
[38] Pierre Sarrazin, Alain Galerie, Jacques Fouletier, Hugh Evans, Mechanisms of High Temperature Corrosion: A Kinetic Approach, Trans Tech Publications Ltd., 2008.
[39] A.S. Khanna, Introduction to High Temperature Oxidation and Corrosion, ASM International, 2002.
[40] M. Soustelle, Cinétique hétérogène : Mécanismes et réactivité, vol. 3, Hermes-Lavoisier, 2006.
[41] G.J. Ackland, A.P. Jones, Phys. Rev. B 73 (2006) 054104.
[42] H. Tsuzuki, P.S. Branicio, J.P. Rino, Comput. Phys. Commun. 177 (2007) 518.
[43] I. Levine, D. Brandon, J. Am. Ceram. Soc. 81 (1998) 1995.